AVITEC
Aviation Electronics, Information Technology, Telecommunications, Electricals, and Controls (AVITEC)
Vol. 8, No. 1, February 2026, pp. 201-213, p-ISSN 2685-2381, e-ISSN 2715-2626
http://dx.doi.org/10.28989/avitec.v8i1.3737

Research Article

Detection of Low Radar Cross Section (RCS) Targets in Sea Clutter Environments using Pulse-Doppler Radar Simulation

Muhammad Rendra Perdana Kusuma Djaka*, Edo Lutfi Mahanani, Muhammad Dhafin Sulaiman AR., Uke Kurniawan Usman
Telecommunication Engineering Study Program, Faculty of Electrical Engineering,
Telkom University, Indonesia.

Article Info

Article history:
Submitted December 25, 2025
Accepted February 9, 2026
Published February 20, 2026

Keywords:
Sea clutter;
pulse-doppler radar;
Constant False Alarm Rate (CFAR);
Ordered-Statistic CFAR (OS-CFAR);
Signal-to-Clutter Ratio (SCR).

ABSTRACT

This paper reports a simulation-based investigation of low-radar-cross-section (low-RCS) maritime target detection using a pulse–Doppler radar operating in K-distributed sea clutter environments. The results indicate that heavy-tailed clutter statistics significantly deteriorate the performance of conventional Cell-Averaging Constant False Alarm Rate (CA-CFAR), particularly under low signal-to-clutter ratio (SCR) and nonhomogeneous clutter conditions. Range–Doppler analysis confirms that coherent Doppler integration and MTI filtering increase target-to-clutter contrast; however, substantial residual clutter persists in rough sea states. A comparative evaluation demonstrates that ordered-statistics CFAR (OS-CFAR) consistently provides superior performance, achieving higher detection probability, enhanced robustness to clutter transitions, stable false alarm regulation, and improved threshold stability. At a detection probability of 0.8, OS-CFAR attains an SCR advantage of approximately 2–3 dB over CA-CFAR under severe clutter conditions. The results further reveal the influence of Doppler ambiguity and blind speed effects, highlighting the necessity of jointly considering detection algorithms and waveform design to achieve reliable maritime radar operation.

Corresponding Author:
Muhammad Rendra Perdana Kusuma Djaka,
Telecommunication Engineering Study Program, Faculty of Electrical Engineering, Telkom University,
West Java, Indonesia.
Email: *muhammadrendra@telkomuniversity.ac.id

1. INTRODUCTION

Maritime radar target detection represents a fundamental challenge in ocean surveillance and naval operations due to the highly stochastic and dynamic nature of the sea surface. The radar return from the sea, commonly referred to as sea clutter, exhibits non-Gaussian statistical properties that are strongly influenced by wind speed, wave height, sea state, and other environmental factors [1][2]. This highly variable backscatter often masks weak or low-observable targets, significantly degrading detection performance. Conventional radar detection algorithms, such as constant false alarm rate (CFAR) detectors, typically assume homogeneous clutter statistics and stationary conditions. These assumptions are often invalid in operational maritime environments, resulting in increased false alarm rates and missed detections [3]. Consequently, the development of robust detection methodologies that can effectively discriminate targets from complex clutter remains a critical research focus.

Correlation-based estimation approaches have been proposed to address the limitations of conventional detection methods. Luo et al. [1] demonstrated that exploiting the spatial and temporal correlation properties of radar returns can enhance the detectability of low-observable targets. By modeling the interdependence between successive radar measurements, correlation-based methods improve signal-to-clutter ratio estimation and provide a statistically grounded mechanism for target identification in high-clutter conditions. Complementary to this, polarimetric radar systems exploit the electromagnetic scattering properties of both targets and the sea surface. Fan et al. [2] showed that full-polarization scattering features significantly improve discrimination between clutter and targets by capturing the vectorial information of scattered fields. Polarimetric analysis, when integrated with adaptive thresholding, provides a powerful tool for reducing false alarms while enhancing sensitivity to weak target signatures.

Adaptive detection techniques further enhance performance by explicitly accounting for non-stationary clutter statistics. Wu et al. [3] investigated adaptive detection in nonzero-mean compound Gaussian sea clutter with random texture, highlighting the critical need for statistical models that incorporate both heavy-tailed distributions and random environmental variability. Such models allow the development of adaptive detectors that dynamically adjust thresholds according to the local clutter environment, thereby mitigating the limitations of fixed-threshold approaches. In a related study, Wang et al. [4] proposed a two-stage collaborative detection framework, combining initial CFAR-based detection with secondary statistical verification to improve detection reliability in nonhomogeneous clutter. These methodologies underscore the importance of integrating adaptive strategies and multi-stage processing to address the intrinsic heterogeneity of maritime radar returns.

The integration of machine learning and deep learning techniques has introduced transformative approaches for maritime radar detection. Wang and Li [5] presented a SALA-LSTM model, a recurrent neural network architecture capable of capturing temporal dependencies in radar echoes. The model effectively differentiates weak targets from clutter by learning latent temporal features that are difficult to model explicitly using conventional statistical techniques. Kandagatla et al. [6] further demonstrated that neural network-based clutter suppression could enhance target detectability by learning non-linear mappings between clutter-dominated input signals and target-enhanced outputs. Al-dabaa et al. [7] combined CFAR detection with intelligent clustering algorithms, achieving improved multiple-target detection in K-distributed clutter by leveraging the complementary strengths of classical statistical detection and data-driven machine learning. These studies indicate that hybrid approaches, which fuse model-based and data-driven methodologies, are highly effective in complex maritime detection scenarios.

Spaceborne synthetic aperture radar (SAR) provides additional capabilities and challenges for maritime surveillance. High-resolution SAR imaging enables detection over large oceanic regions, but it also increases sensitivity to clutter and environmental variability. For small targets immersed in heavy-tailed sea clutter, robust CFAR design is critical. Dong et al. [8] developed a CFAR detector tailored for K-distributed clutter, demonstrating improved robustness against clutter spikes compared to conventional methods. Moreover, rigorous statistical methods, such as the complex parameter Rao and Wald tests, allow quantitative assessment of covariance structures in radar returns, facilitating robust performance evaluation under uncertain conditions [9]. These analytical frameworks provide critical tools for validating detection algorithms and ensuring operational reliability.

Spectral and spatio-temporal domain approaches have also emerged as effective mechanisms for enhancing target detection. Liu et al. [10] proposed a spectral mode reconstruction technique that separates target signals from sea clutter based on frequency-domain characteristics, effectively enhancing weak target signatures. Wen et al. [11] developed a spatio-temporal joint filtering approach for sequential radar imagery, which leverages both spatial correlations and temporal continuity to suppress clutter and improve target visibility. Such approaches are particularly beneficial for detecting moving targets and those exhibiting subtle motion, which often remain obscured in conventional single-frame processing methods.

Environmental variability, including abnormal weather and dynamic sea states, introduces additional complexity into target detection. Bounaceur et al. [12] analyzed small sea-surface target detection under adverse weather conditions, revealing that adaptive processing algorithms are essential to maintain performance when conventional methods fail. Xue et al. [13] proposed an adaptive persymmetric detection framework for correlated CG-LN sea clutter, demonstrating robustness in highly nonhomogeneous and temporally correlated clutter environments. These findings highlight the critical importance of adaptive detection strategies that respond to both spatial and temporal variations in the radar clutter environment.

Empirical validation of detection methodologies remains vital to ensure theoretical developments translate to operational capability. Zhang et al. [14] conducted experimental investigations using Ka-band radar with meter-level resolution over the Yellow Sea, providing evidence that high-resolution radar measurements significantly improve target discrimination while capturing detailed clutter characteristics. Such experimental results underscore the necessity of integrating high-resolution sensing, advanced signal processing, and adaptive detection strategies for effective maritime surveillance.

Despite the advancements in maritime radar detection techniques reviewed above [1]–[14], a significant gap persists in the quantitative evaluation and direct comparison of adaptive CFAR detectors under a high-fidelity, end-to-end simulation environment that accurately replicates the non-Gaussian statistics of sea clutter. While studies have employed adaptive detection frameworks [3][13] and evaluated specific detectors [7][8], a comprehensive analysis using a fully coherent Pulse-Doppler radar simulation integrating Swerling target fluctuations, realistic clutter generation via the Spherically Invariant Random Process (SIRP), MTI filtering, Doppler processing, and culminating in a Range-Doppler Map remains limited. Furthermore, a clear quantification of the processing gain offered by robust detectors like OS-CFAR over CA-CFAR in such a controlled yet realistic setting is needed to guide system design, building upon foundational CFAR theory [15] and maritime radar principles [16].

This study aims to bridge this gap between high-fidelity simulation and robust detection theory. The primary contributions of this paper are threefold: (1) the development of a comprehensive Pulse-Doppler radar simulation framework ('Virtual Testbench') that generates realistic K-distributed sea clutter via the SIRP method and Swerling I target returns; (2) a rigorous comparative performance analysis of CA-CFAR and OS-CFAR detectors across multiple sea states (varying shape parameter ν) using this framework, explicitly evaluating the masking effect and false alarm regulation, extending the seminal work on OS-CFAR [17]; and (3) the quantification of a concrete processing gain in Signal-to-Clutter Ratio (SCR) achieved by OS-CFAR, providing a reproducible benchmark for detector performance in complex maritime environments.

Although neither the OS-CFAR algorithm nor the K-distribution clutter model is novel when considered independently, the novelty of this work lies in their systematic integration and quantitative evaluation within a coherent, end-to-end Pulse-Doppler radar simulation pipeline tailored for low-RCS maritime target detection. By embedding robust statistical detection into a high-fidelity virtual testbench that incorporates realistic clutter generation, Doppler processing, and controlled sea-state variability, this study provides practical insights and reproducible performance benchmarks that are not sufficiently addressed in existing literature.

2. RESEARCH METHOD

This chapter presents the complete research methodology used to develop a high-fidelity Virtual Testbench for evaluating low Radar Cross Section (RCS) maritime target detection in heavy sea clutter environments. The proposed framework integrates realistic radar system parameters, statistically accurate sea clutter modeling, coherent Pulse–Doppler signal processing, and adaptive CFAR-based detection. The primary objective is to ensure methodological clarity, reproducibility, and a fair comparative evaluation of CA-CFAR and OS-CFAR detectors under controlled yet realistic maritime conditions. The research methodology is organized into five main components:

1. Radar System Parameters and Simulation Configuration
2. Radar Scene and Target Modeling
3. Sea Clutter and Noise Modeling
4. Digital Pulse–Doppler Radar Signal Processing
5. Detection Algorithm Configuration and Performance Evaluation.

2.1 Radar System Parameters and Simulation Configuration

The radar system is configured to emulate a practical maritime surveillance radar operating in the X-band. All parameters used in the simulation are summarized in Table 1 to ensure full reproducibility of the results.

The simulated radar operates at a carrier frequency of 10 GHz, corresponding to a wavelength of 0.03 m. A peak transmit power of 5 kW and an antenna gain of 30 dB are selected to represent a realistic surface surveillance radar capable of illuminating low-RCS maritime targets. The pulse width is set to 1 μs with a signal bandwidth of 10 MHz, yielding a theoretical range resolution of approximately 15 m after pulse compression. These parameters provide a balanced trade-off between spatial resolution, sea clutter sensitivity, and practical system constraints.

The pulse repetition frequency (PRF) is fixed at 2 kHz to allow sufficient Doppler sampling while maintaining acceptable unambiguous range performance. Each coherent processing interval (CPI) consists of 64 pulses, resulting in a CPI duration of 32 ms. This configuration enables coherent Doppler processing with a theoretical integration gain of approximately 18 dB and provides adequate velocity resolution for separating slow-moving maritime targets from Doppler-spread sea clutter.

2.2 Radar Scene and Target Modeling

The simulated radar scene represents a maritime environment containing a single moving low-observable surface target embedded in heterogeneous sea clutter. Both deterministic radar physics and stochastic target fluctuations are incorporated to emulate realistic operational conditions.

2.2.1 Target Scattering and RCS Fluctuation

To capture realistic target echo variability, the target radar cross section is modeled using the Swerling Case I fluctuation model. In this model, the target RCS remains constant within a single CPI but varies independently between CPIs, which is appropriate for small maritime targets such as periscopes, floating objects, or small unmanned vessels. The received complex baseband signal corresponding to one transmitted pulse is expressed as Equation (1).

Table 1. Radar and Simulation Parameters

Parameter	Symbol	Value	Unit	Description/Rationale
Transmit Power	Pt	5	kW	Typical peak transmit power for X/Ku-band maritime surveillance radar, ensuring sufficient illumination of low-RCS targets
Antenna Gain	G	30	dB	Represents a moderately high-gain directional antenna commonly used in surface surveillance radar
Carrier Frequency	fc	10	GHz	Selected to emulate X-band maritime radar, providing a trade-off between resolution and sea clutter sensitivity
Wavelength	λ	0.03	m	Derived from carrier frequency (λ = c / fc)
Pulse Width	τp	1	μs	Enables fine range resolution while maintaining sufficient transmitted pulse energy
Signal Bandwidth	B	10	MHz	Provides high range resolution after pulse compression
Pulse Repetition Frequency	PRF	2	kHz	Selected to balance unambiguous range and Doppler coverage
Number of Pulses per CPI	M	64	pulses	Ensures sufficient coherent integration gain and Doppler resolution
Coherent Processing Interval	CPI	32	ms	Computed as M / PRF, ensuring phase coherence during Doppler processing
Range Resolution	ΔR	15	m	Computed as c / (2B), consistent with high-resolution radar systems
Doppler Resolution	Δfd	PRF / M	Hz	Determines velocity discrimination capability in Doppler processing
Target Radar Cross Section	σ	0.1 – 1.0	m²	Represents low-observable maritime targets such as small vessels or periscopes
Target Fluctuation Model	—	Swerling I	—	Models scan-to-scan RCS variability typical of maritime targets
Sea Clutter Model	—	K-distribution	—	Captures heavy-tailed, non-Gaussian sea clutter characteristics
Clutter Shape Parameter	ν	0.5 – 2.0	—	Represents varying sea states from rough (low ν) to calm (high ν) conditions
Clutter Generation Method	—	SIRP	—	Separates texture and speckle components for realistic clutter synthesis
Noise Model	—	AWGN	—	Models receiver thermal noise
CFAR Reference Cells	N	24	cells	Provides reliable clutter statistics while limiting edge effects
CFAR Guard Cells	Gc	4	cells	Prevents target signal leakage into the reference window
CA-CFAR Threshold Scaling	αCA	Adaptive	—	Automatically adjusted to maintain the desired false alarm probability
OS-CFAR Rank Selection	k	75th percentile	—	Rejects strong clutter spikes to improve robustness in non-homogeneous environments
False Alarm Probability	Pfa	1×10^{-4}	—	Typical operational false alarm requirement for maritime radar
Monte Carlo Trials	NMC	100,000	runs	Ensures statistical reliability of detection and false alarm performance

$$s_{target}(t) = \sqrt{P_r} \cdot \alpha \cdot rect(\frac{t-\tau}{\tau_p}) e^{j(2\pi f_d t + \phi_0)} \quad (1)$$

where: P_r : received signal power
α : a Rayleigh-distributed complex scattering coefficient representing target fluctuation
$\tau = 2R/c$: round-trip propagation delay for a target at range R
τ_p : pulse width
$f_d = 2v_r/\lambda$: Doppler frequency shift associated with the target radial velocity v_r
λ : radar wavelength
ϕ_0 : initial carrier phase.

The received power P_r follows the monostatic radar Equation (2).

$$P_r = \frac{P_t G^2 \lambda^2 \sigma}{(4\pi)^3 R^4 L} \quad (2)$$

where: P_t : the peak transmit power
G : antenna gain
σ : target radar cross section
L : represents system losses.

The target RCS is varied between 0.1 m^2 and 1.0 m^2 to represent low-observable maritime threats.

2.3 Sea Clutter and Noise Modeling

2.3.1 K-Distributed Sea Clutter Model

Sea clutter in high-resolution maritime radar systems exhibits strong non-Gaussian behavior due to wave breaking, multipath scattering, and surface roughness variability. To accurately model this behavior, sea clutter amplitude is described using the K-distribution, whose probability density function is given by Equation (3).

$$p(E) = \frac{2}{a\Gamma(\nu)}\left(\frac{E}{2a}\right)^{\nu} K_{\nu-1}\left(\frac{E}{a}\right) \quad (3)$$

where: E : clutter envelope amplitude
a : scale parameter
ν : shape parameter controlling clutter spikiness
$\Gamma(\cdot)$: Gamma function
$K_{\nu-1}(\cdot)$: modified Bessel function of the second kind.

Lower values of νcorrespond to rough sea conditions characterized by highly spiky clutter. To synthesize K-distributed clutter, the Spherically Invariant Random Process (SIRP) model is employed by Equation (4).

$$c_{sea} = \sqrt{g} \cdot z(t) \quad (4)$$

where: g : Gamma-distributed texture component representing slow-varying sea surface modulation
$z(t)$: zero-mean complex Gaussian speckle component representing fast-varying scattering.

To evaluate detector robustness under different environmental conditions, the clutter shape parameter $\nu$is varied from 0.5 to 2.0. A value of $\nu = 0.5$ represents rough sea conditions with pronounced heavy-tailed behavior, whereas higher values correspond to calmer sea states.

2.3.2 Thermal Noise Modeling

The receiver noise is modeled as Additive White Gaussian Noise (AWGN), which represents thermal noise generated by random electron motion within the receiver circuitry. Statistically, the noise is assumed to be a zero-mean Gaussian random process with variance N_0, expressed as Equation (5).

$$n(t) \sim \mathcal{N}(0, N_0) \quad (5)$$

The AWGN model assumes that the noise is additive, spectrally white over the bandwidth of interest, and Gaussian distributed due to the aggregation of numerous independent random processes.

Accordingly, the total received complex baseband signal can be represented as the superposition of the target signal, sea clutter, and receiver noise as in Equation (6).

$$x(t) = s_{\text{target}}(t) + c_{\text{sea}}(t) + n(t) \quad (6)$$

where: $s_{\text{target}}(t)$: desired target return
$c_{\text{sea}}(t)$: interference caused by sea surface reflections
$n(t)$: thermal noise component.

This signal model forms the basis for performance analysis and target detection algorithms.

2.4 Digital Radar Processing

The received signal is processed using a coherent digital Pulse–Doppler radar receiver chain, as commonly employed in modern maritime surveillance systems. Coherent processing preserves the phase information of the received echoes, which is essential for accurate range and Doppler estimation.

2.4.1 Matched Filtering and Pulse Compression

Pulse compression is achieved by applying a matched filter whose impulse response is the complex conjugate time-reversed replica of the transmitted waveform. The matched filtering operation is expressed as Equation (7).

$$y(t) = x(t) * h^*(T - t) \quad (7)$$

where: $x(t)$: the received complex baseband signal
$h(t)$: the transmitted pulse
T : pulse duration
* represents convolution.

This process correlates the received signal with the transmitted waveform, resulting in temporal compression of the pulse.

Matched filtering maximizes the output signal-to-noise ratio in the presence of additive white Gaussian noise. The corresponding processing gain is approximately equal to the time-bandwidth product of the transmitted signal as in Equation (8).

$$G_p \approx \tau_p B \quad (8)$$

where: τ_p : pulse duration
B : signal bandwidth.

This gain enables improved range resolution while maintaining high transmitted energy.

2.4.2 Moving Target Indication

To suppress low-Doppler sea clutter, a three-pulse Moving Target Indication (MTI) canceller is applied, with the transfer function as expressed by Equation (9).

$$H(z) = 1 - 2z^{-1} + z^{-2} \quad (9)$$

This filter attenuates stationary and slow-moving clutter while preserving moving target echoes. Staggered PRFs are employed to mitigate blind-speed effects.

2.4.3 Doppler Processing

Doppler processing is performed by applying an M-point Fast Fourier Transform (FFT) across the slow-time dimension for each range bin. The discrete Doppler spectrum is obtained as Equation (10).

$$Y(k) = \sum_{n=0}^{M-1} y[n] e^{-j\frac{2\pi}{M}nk} \quad (10)$$

where: $y[n]$: the matched-filter output sequence over successive pulses
M : the number of coherent pulses
k : the Doppler bin index.

This operation produces a Range–Doppler Map (RDM), enabling target discrimination based on radial velocity.

The coherent integration achieved through Doppler processing provides a theoretical signal-to-noise ratio (SNR) gain proportional to the number of integrated pulses, which can be expressed as Equation (11).

$$SNR_{gain} = 10log_{10}(M)\ dB \quad (11)$$

This gain improves target detectability, particularly for weak moving targets in noise- and clutter-dominated maritime environments.

2.5 Detection Algorithm Configuration and Performance Evaluation

Both CA-CFAR and OS-CFAR detectors employ identical guard and reference window configurations to ensure a fair comparison. The number of reference cells is fixed at 24, with 4 guard cells on each side of the cell under test to prevent target leakage. The desired false alarm probability is set to $P_{fa} = 10^{-4}$, which reflects a typical operational requirement for maritime surveillance systems.

2.5.1 Cell-Averaging CFAR (CA-CFAR)

CA-CFAR estimates background power by averaging $2N$ reference cells surrounding the cell under test (CUT) as in Equation (12).

$$Z_{CA} = \frac{1}{2N} \sum_{j=1}^{2N} x_j \quad (12)$$

A target is declared present when $x(i) \geq \alpha_{\mathrm{CA}} Z_{\mathrm{CA}}$, where α_{CA} is the threshold scaling factor determined by the desired false alarm probability.

2.5.2 Ordered-Statistic CFAR (OS-CFAR)

OS-CFAR improves robustness in non-homogeneous clutter by sorting the reference samples and selecting the k-th ordered statistic as in Equation (13).

$$Z_{OS} = x_{(k)} \quad (13)$$

Detection occurs when $x(i) \geq \alpha_{\mathrm{OS}} x_{(k)}$. The rank index is selected at the 75th percentile of the ordered reference samples, effectively rejecting high-amplitude clutter spikes while maintaining sensitivity to weak targets.

2.5.3 Performance Evaluation Methodology

Detector performance is evaluated using Monte Carlo simulations with 10^5 independent trials per scenario. The probability of detection is computed as Equation (14).

$$P_d = \frac{N_{detect}}{N_{trials}} \quad (14)$$

Statistical validation of the clutter model is performed by comparing empirical amplitude histograms obtained from the simulated sea clutter with the theoretical K-distribution probability density function. The close agreement between simulated and theoretical distributions confirms the validity of the SIRP-based clutter generation approach.

3. RESULTS AND DISCUSSION

This section presents a comprehensive analysis of the simulation results obtained using the proposed pulse–Doppler radar framework for detecting low-RCS maritime targets embedded in K-distributed sea clutter. The discussion emphasizes the physical interpretation of the results, statistical behavior of clutter, effectiveness of Doppler and MTI processing, and the comparative performance of CA-CFAR and OS-CFAR detectors under challenging maritime conditions.

3.1 Signal and Clutter Characteristics Validation

Figure 1 illustrates a representative received radar signal composed of the coherent target return embedded in additive receiver noise. The oscillatory structure observed in the signal corresponds to the Doppler-induced phase modulation caused by target motion, while the random fluctuations represent thermal noise contributions. Although target detection is not directly feasible in the time domain, this result confirms that the simulated signal preserves coherent Doppler information prior to frequency-domain processing.

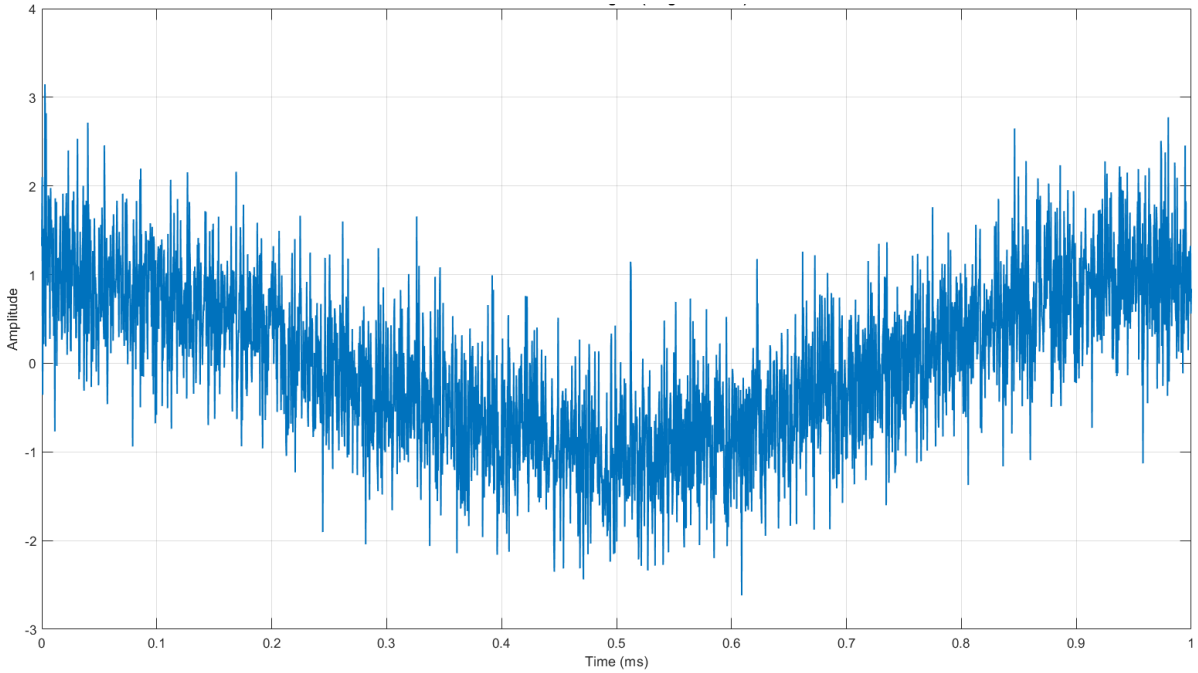

Figure 1. Received Radar Signal (Target + Noise)

Figure 2 presents the statistical validation of the synthesized sea clutter. The empirical amplitude distributions obtained via Monte Carlo simulations are compared with the theoretical K-distribution probability density functions for different values of the shape parameter ν. For rough sea conditions ($\nu = 0.5$), the clutter exhibits pronounced heavy-tailed behavior, indicating frequent high-amplitude clutter spikes. As νincreases toward 2.0, the distribution progressively approaches a Rayleigh-like shape associated with calmer sea states.

The close agreement between empirical histograms and theoretical distributions confirms the accuracy of the adopted SIRP-based clutter generation model. This validation is critical because CFAR detector performance is highly sensitive to clutter statistics. Any deviation from the assumed distribution may significantly bias threshold estimation and compromise detection reliability.

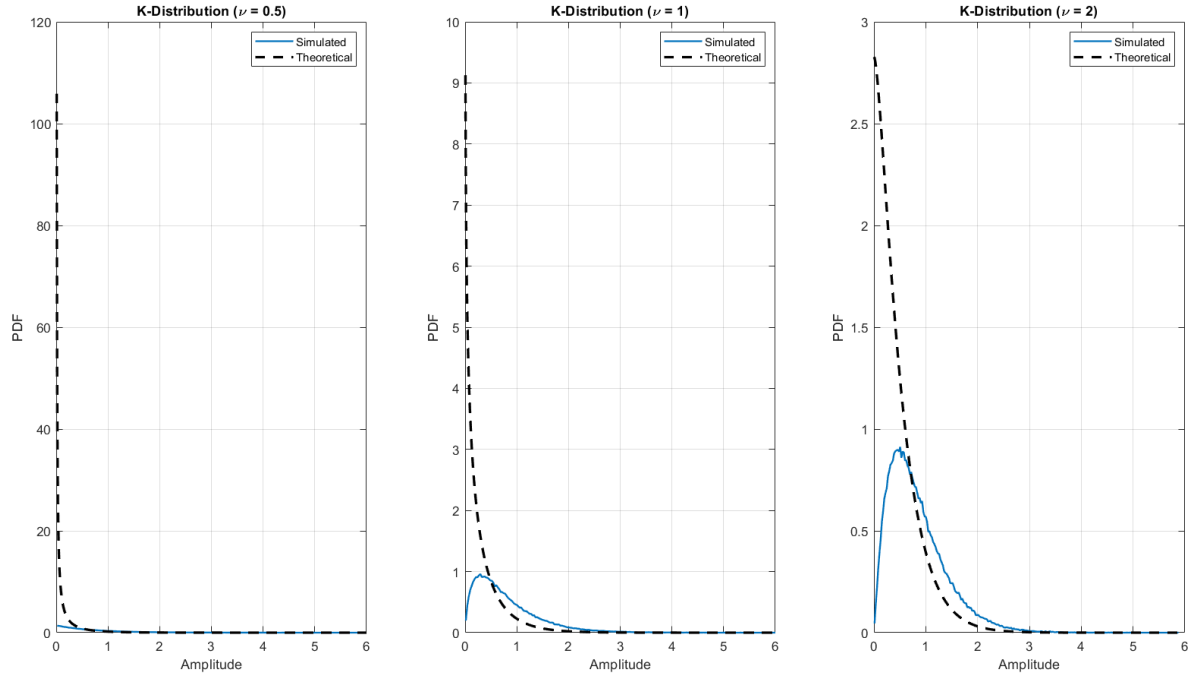

Figure 2. K-Distributed Sea Clutter Statistics

3.2 Range–Doppler Representation under K-Distributed Sea Clutter

Figure 3 shows the range–Doppler map obtained after coherent Doppler processing in the presence of K-distributed sea clutter. The clutter energy is predominantly concentrated around zero Doppler frequency, reflecting the slow and quasi-stationary motion of sea surface scatterers. This behavior is consistent with physical maritime environments, where most clutter returns originate from waves with low radial velocity relative to the radar.

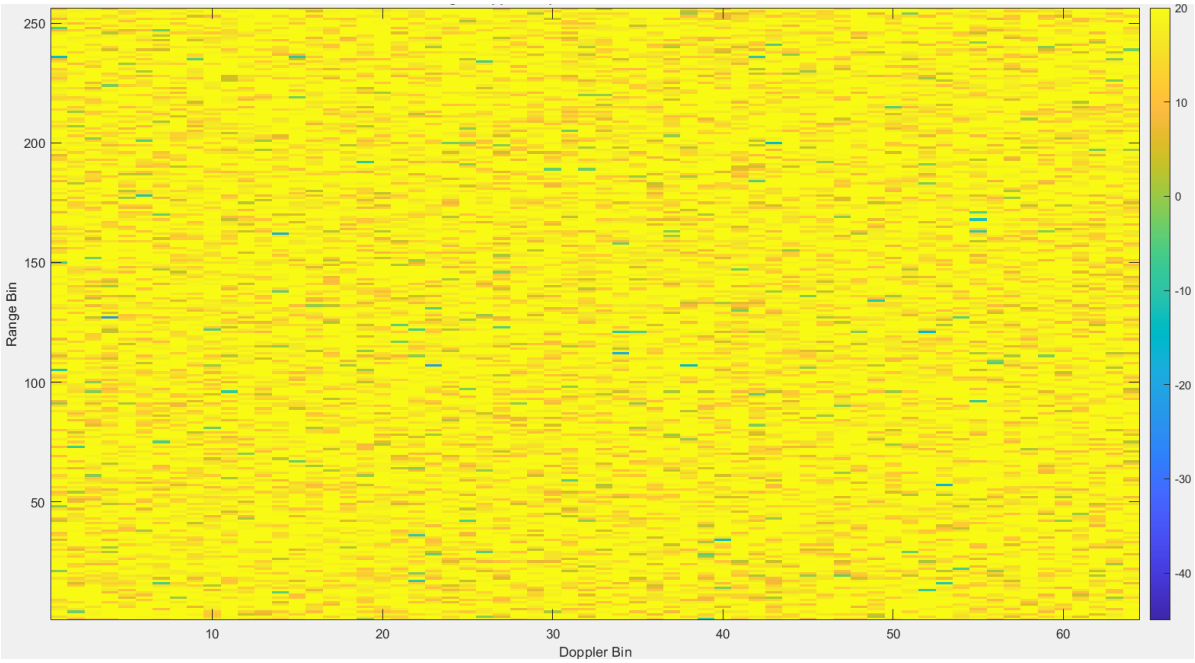

Figure 3. Range–Doppler Map under K-Distributed Sea Clutter

Despite the coherent integration gain, the low-RCS target response remains partially masked by clutter sidelobes under rough sea conditions. This highlights a fundamental limitation of Doppler processing alone when operating in non-Gaussian clutter environments. While coherent integration enhances signal energy, it does not sufficiently suppress heavy-tailed clutter components.

Figure 4 compares the range–Doppler maps before and after MTI filtering. The application of MTI significantly suppresses low-Doppler clutter components, resulting in a clearer separation between the target and clutter. After MTI filtering, the target signature becomes more prominent, particularly in the Doppler dimension.

However, residual clutter remains due to the nonstationary nature of sea clutter and the limited rejection capability of finite-order MTI filters. This observation motivates the need for adaptive detection strategies.

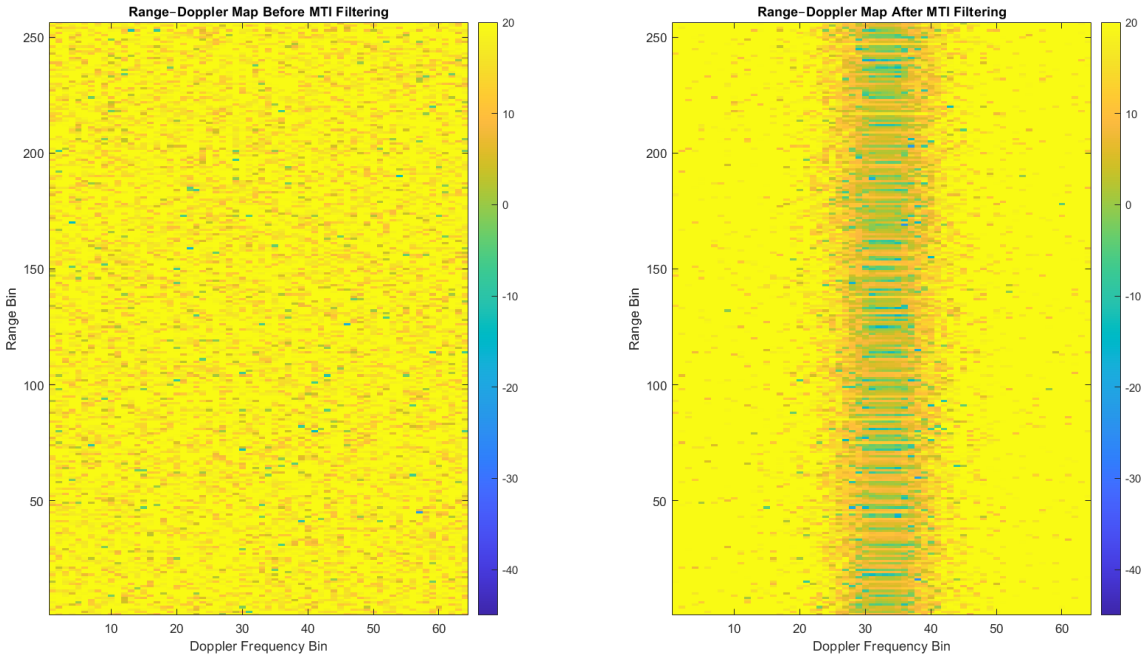

Figure 4. Range–Doppler Map before and after MTI Filtering

3.3 Detection Performance versus Signal-to-Clutter Ratio

The detection performance of CA-CFAR and OS-CFAR detectors is evaluated in Figure 5, which plots the probability of detection ($\boldsymbol{P_d}$) as a function of signal-to-clutter ratio (SCR) at a fixed false alarm probability of $P_{fa} = 10^{-4}$. Under moderately homogeneous clutter conditions, both detectors exhibit similar detection performance. As the clutter becomes increasingly heavy-tailed, CA-CFAR performance degrades significantly, particularly in low-SCR regimes. This degradation arises from the averaging operation used in CA-CFAR, which is highly sensitive to extreme clutter outliers within the reference window. In contrast, OS-CFAR demonstrates superior robustness by selecting a ranked reference cell, thereby suppressing the influence of high-amplitude clutter spikes. At a detection probability of $P_d = 0.8$, OS-CFAR achieves an SCR improvement of approximately 2–3 dB compared to CA-CFAR under rough sea conditions. This gain is operationally significant, as it translates to extended detection range or improved sensitivity to weak targets.

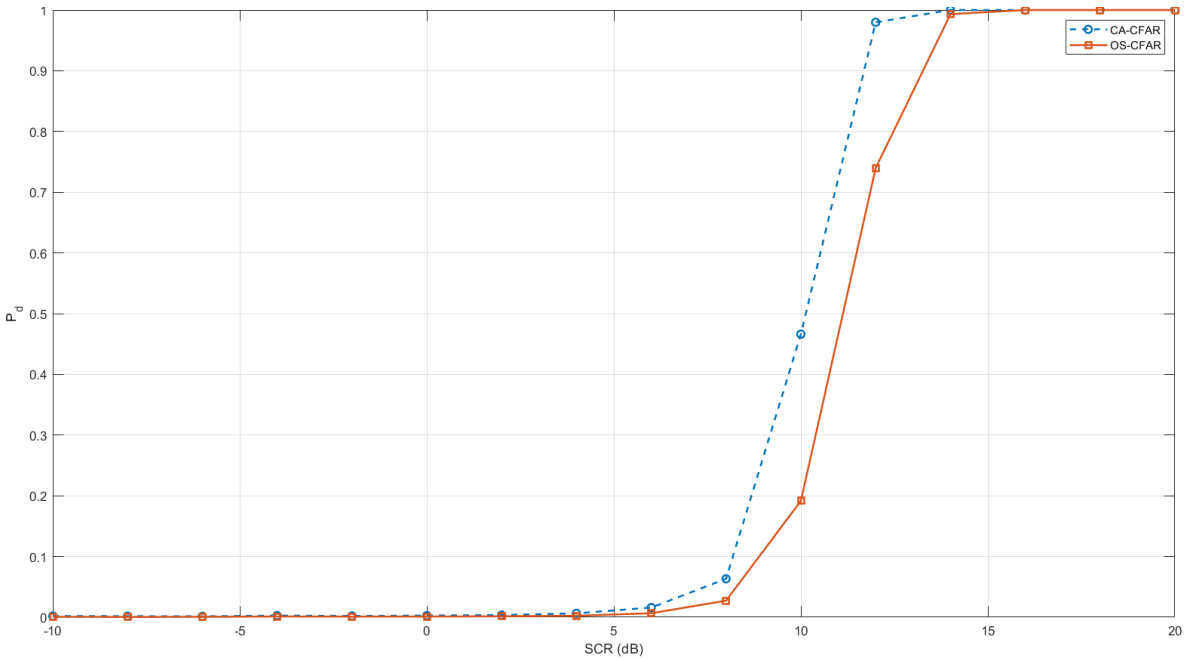

Figure 5. Detection Probability versus SCR

3.4 Impact of Target RCS and Doppler Frequency

Figure 6 illustrates the false alarm behavior of both detectors in the presence of spatially nonhomogeneous clutter, such as clutter edges or localized interference regions. CA-CFAR exhibits pronounced false alarm spikes near clutter transitions due to biased clutter power estimation caused by reference cell contamination. OS-CFAR demonstrates superior robustness in these scenarios by selecting a lower-ranked reference cell that is less affected by localized clutter power variations. As a result, OS-CFAR maintains a relatively stable false alarm probability across the transition region. This characteristic is particularly important in maritime radar applications, where sea state variations and environmental changes frequently lead to nonhomogeneous clutter conditions.

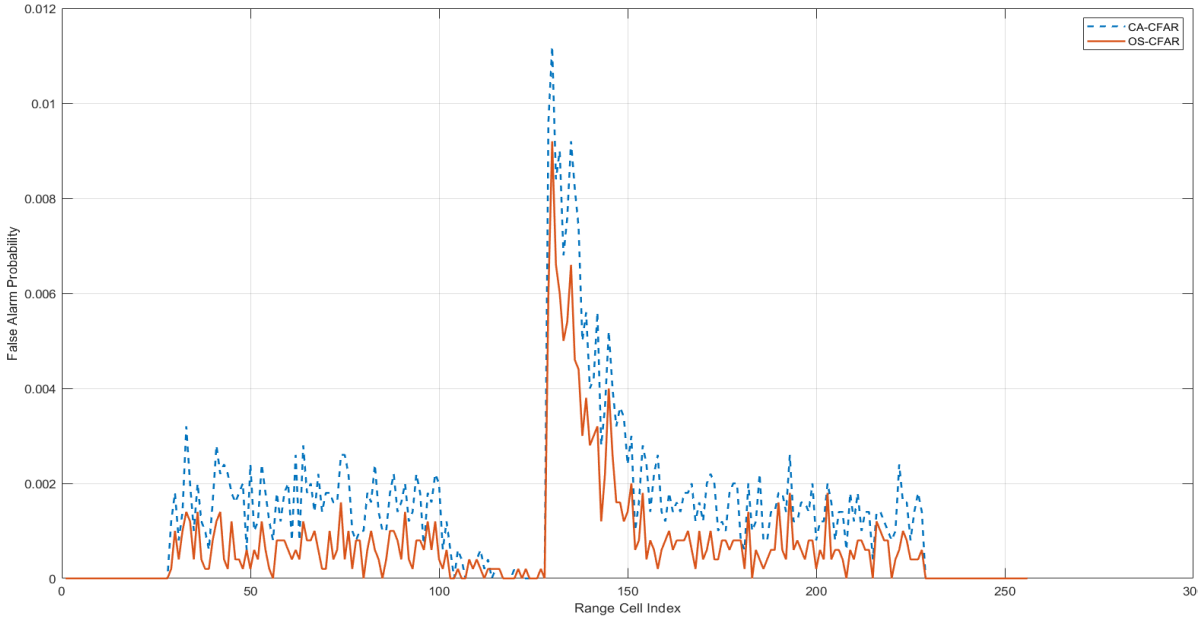

Figure 6. False alarm behavior at clutter transition

3.5 Impact of Target Radar Cross Section

The influence of target radar cross section (RCS) on detection performance is examined in Figure 7. As expected, detection probability increases with increasing RCS for both CFAR detectors. However, detection performance degrades significantly for low-RCS targets, particularly when the target's Doppler frequency is close to zero. Despite these challenges, OS-CFAR consistently outperforms CA-CFAR across the entire RCS range. This robustness is especially important for maritime surveillance systems tasked with detecting small vessels, periscopes, or floating debris with limited radar reflectivity.

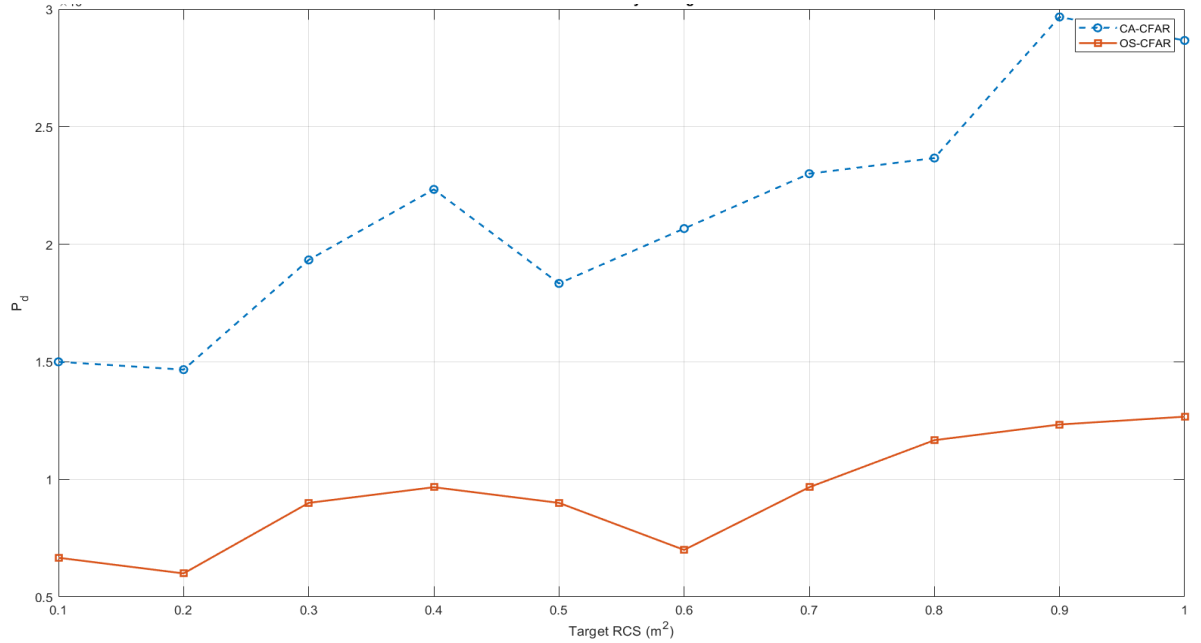

Figure 7. Detection Probability versus Target RCS

3.6 Receiver Operating Characteristic Analysis

Figure 8 presents the receiver operating characteristic (ROC) curves for CA-CFAR and OS-CFAR under heavy sea clutter conditions. The ROC curves illustrate the trade-off between detection probability and false alarm probability over a wide operating range. For a given false alarm probability, OS-CFAR consistently achieves higher detection probability than CA-CFAR. This advantage becomes increasingly pronounced at low false alarm rates, which are typically required in operational radar systems. The ROC analysis confirms the superior detection–false alarm trade-off provided by OS-CFAR in non-Gaussian clutter environments.

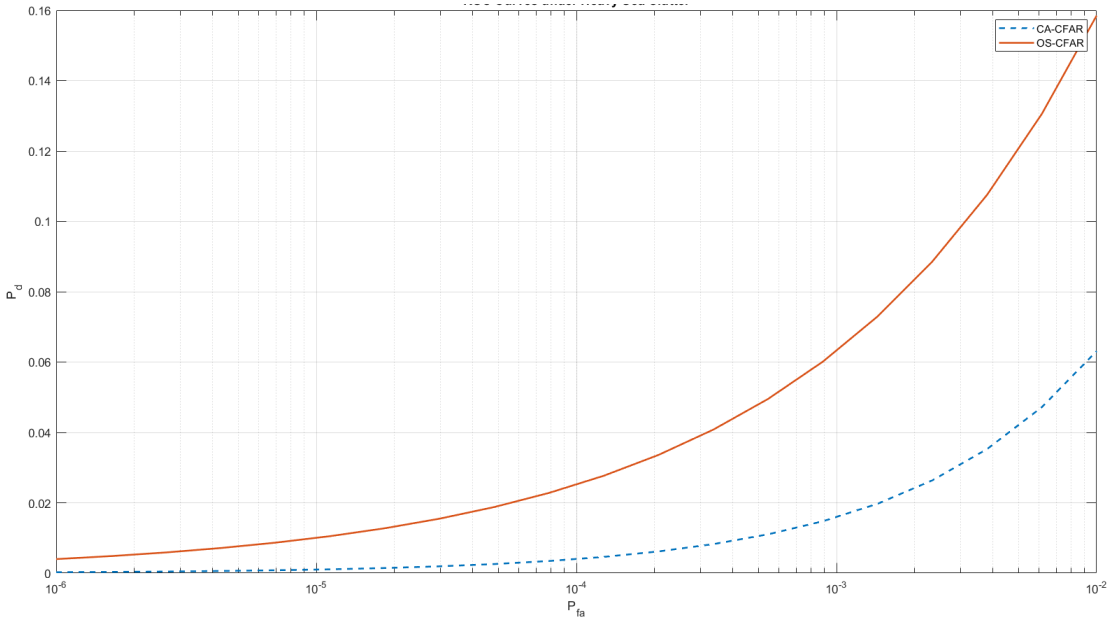

Figure 8. ROC Curves under Heavy Sea Clutter

3.7 CFAR Threshold Stability Analysis

Figure 9 illustrates the spatial variation of CFAR detection thresholds across range cells in a nonstationary clutter environment. CA-CFAR thresholds exhibit significant fluctuations due to sensitivity to clutter power variations, leading to unstable detection behavior. In contrast, OS-CFAR produces smoother and more stable threshold profiles, reflecting its reduced sensitivity to extreme clutter samples. Threshold stability is a critical requirement for reliable radar operation, as unstable thresholds may result in intermittent detections or excessive false alarms. The results clearly demonstrate the superiority of OS-CFAR in maintaining detection reliability under realistic maritime clutter conditions.

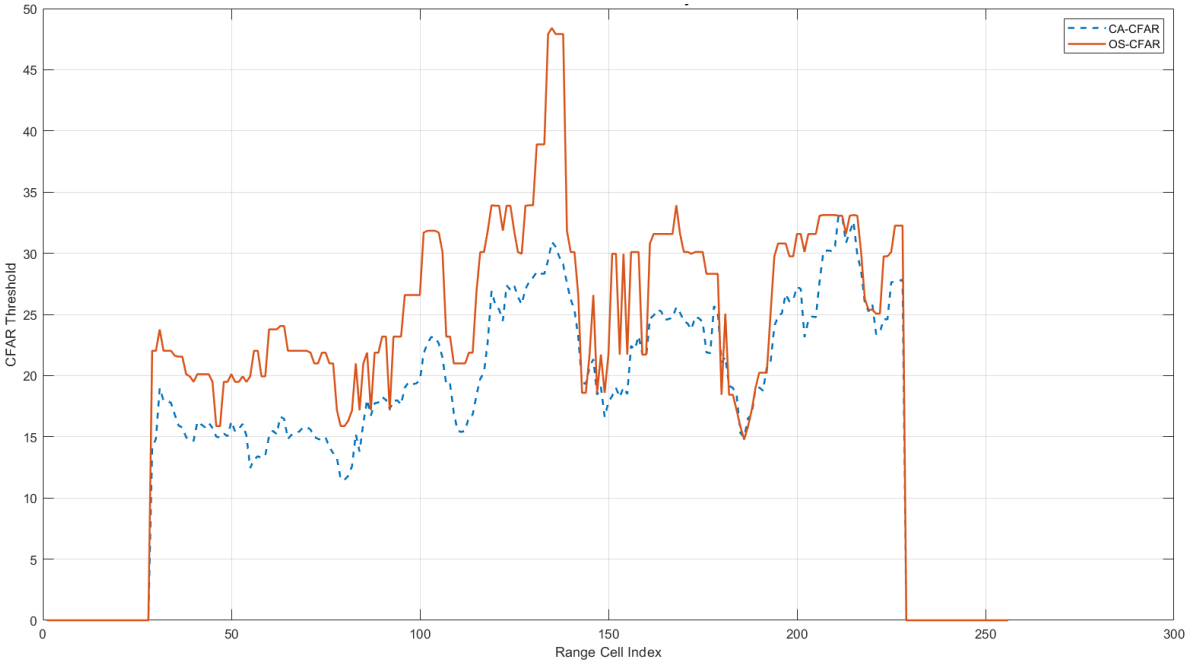

Figure 9. CFAR Threshold Stability

4. CONCLUSION

This work has presented a comprehensive simulation-based investigation of low-radar-cross-section (low-RCS) maritime target detection using a coherent pulse–Doppler radar operating in K-distributed sea clutter environments. The results confirm that although coherent Doppler integration and MTI filtering provide meaningful enhancement of target-to-clutter contrast, these front-end processing stages alone are insufficient to guarantee reliable detection in the presence of heavy-tailed, non-Gaussian clutter. Conventional CA-CFAR is shown to suffer substantial performance degradation under such conditions due to its inherent sensitivity to clutter outliers and nonhomogeneous background statistics, leading to reduced detection probability and unstable false alarm behavior, particularly in rough sea states and clutter transition regions. In contrast, OS-CFAR demonstrates consistently superior robustness across all evaluated scenarios, achieving higher detection probability at low signal-to-clutter ratios, improved resilience to spatial clutter nonhomogeneity, smoother threshold behavior, and more stable false alarm regulation. The observed SCR gain of approximately 2–3 dB at moderate-to-high detection probability represents a practically significant improvement for the detection of weak and low-observable maritime targets. The analysis further highlights the impact of Doppler ambiguity and blind-speed phenomena, underscoring the necessity of jointly considering waveform design and detection strategy in system-level optimization. Overall, the findings establish robust CFAR processing particularly OS-CFAR as a critical enabling technology for maritime radar systems operating in heavy-tailed clutter, while the proposed high-fidelity simulation framework offers a reproducible and extensible platform for future research incorporating real clutter measurements, adaptive waveform optimization, and learning-assisted clutter mitigation techniques.

REFERENCE

[1] Z. Luo, Z. Li, C. Zhang, J. Deng, and T. Qin, "Low observable radar target detection method within sea clutter based on correlation estimation," *Remote Sensing*, vol. 14, no. 9, art. no. 2233, 2022. https://doi.org/10.3390/rs14092233

[2] Y. Fan *et al*., "Weak target detection based on full-polarization scattering features under sea clutter background," *Remote Sensing*, vol. 16, no. 16, art. no. 2987, 2024. https://doi.org/10.3390/rs16162987

[3] H. Wu, Z. Wang, H. Guo, and Z. He, "Adaptive radar target detection in nonzero-mean compound Gaussian sea clutter with random texture," *Signal Processing*, vol. 227, art. no. 109720, 2025. https://doi.org/10.1016/j.sigpro.2024.109720

[4] J. Wang, T. Xiao, and P. Liu, "Radar target detection in sea clutter based on two-stage collaboration," *Journal of Marine Science and Engineering*, vol. 13, no. 8, art. no. 1556, 2025. https://doi.org/10.3390/jmse13081556

[5] J. Wang and S. Li, "SALA-LSTM: A novel high-precision maritime radar target detection method based on deep learning," *Scientific Reports*, vol. 13, no. 1, art. no. 12125, 2023. https://doi.org/10.1038/s41598-023-39348-3

[6] R. K. Kandagatla, V. Malapati, K. Cherukuri, B. Sindhe, V. K. Padarti, and B. K. Thammileti, "Sea clutter suppression using neural network," *Maritime Technology and Research*, vol. 7, no. 1, art. no. 270067, 2025. https://doi.org/10.33175/mtr.2025.272334

[7] M. M. Al-Dabaa, E. Laslo, A. A. Emran, A. Yahya, and A. Aboshosha, "Multiple-target CFAR detection performance based on an intelligent clustering algorithm in K-distribution sea clutter," *Sensors*, vol. 25, no. 8, art. no. 2613, 2025. https://doi.org/10.3390/s25082613

[8] Y. Dong, C. Wang, and J. Li, "A robust CFAR detector for small targets in sea clutter with K-distribution," *IEEE Transactions on Aerospace and Electronic Systems*, vol. 58, no. 3, pp. 1925–1937, Jun. 2022. https://doi.org/10.1109/TAES.2021.3120914

[9] Z. Zhu, "Complex parameter Rao and Wald tests for assessing the bandedness of a complex-valued covariance matrix," *Signals*, vol. 5, no. 1, pp. 1–17, 2024. https://doi.org/10.3390/signals5010001

[10] N. Liu, H. Yang, G. Wang, H. Ding, Y. Dong, and W. Xue, "A spectral mode reconstruction method for floating target detection under strong sea clutter conditions," *Remote Sensing*, vol. 17, no. 18, art. no. 3155, 2025. https://doi.org/10.3390/rs17183155

[11] B. Wen, Y. Wei, and Z. Lu, "Sea clutter suppression and target detection algorithm of marine radar image sequence based on spatio-temporal domain joint filtering," *Entropy*, vol. 24, no. 2, art. no. 250, 2022. https://doi.org/10.3390/e24020250

[12] H. Bounaceur, A. Khenchaf, and J.-M. Le Caillec, "Analysis of small sea-surface target detection performance according to airborne radar parameters in abnormal weather environments," *Sensors*, vol. 22, no. 9, art. no. 3263, 2022. https://doi.org/10.3390/s22093263

[13] J. Xue, H. Li, M. Pan, and J. Liu, "Adaptive persymmetric detection for radar targets in correlated CG-LN sea clutter," *IEEE Transactions on Geoscience and Remote Sensing*, vol. 61, pp. 1–12, 2023. https://doi.org/10.1109/TGRS.2023.3303861

[14] X. Zhang, X. Su, L. Liu, and Z. Wu, "Experimental investigation of meter-level resolution radar measurement at Ka-band in the Yellow Sea," *Remote Sensing*, vol. 16, no. 20, art. no. 3835, 2024. https://doi.org/10.3390/rs16203835

[15] X. Meng, "Rank-sum nonparametric CFAR detector in nonhomogeneous background," *IEEE Transactions on Aerospace and Electronic Systems*, vol. 57, no. 1, pp. 397–403, Jan. 2021. https://doi.org/10.1109/TAES.2020.3017319

[16] M. T. Silva, W. Huang, and E. W. Gill, "Bistatic high-frequency radar cross-section of the ocean surface with arbitrary wave heights," *Remote Sensing*, vol. 12, no. 4, art. no. 667, Feb. 2020. https://doi.org/10.3390/rs12040667

[17] H. Rohling, "Radar CFAR thresholding in clutter and multiple-target situations," *IEEE Transactions on Aerospace and Electronic Systems*, vol. AES-19, no. 4, pp. 608–621, Jul. 1983. https://doi.org/10.1109/TAES.1983.309350